Supplementary Movie Legends

Movie S1. Growth of wild-type *C. crescentus* cells. Phase contrast images were collected every 15 minutes for 6 hours. Scale bar is 1 μm. Corresponds to Fig. 1A, left panel.

Movie S2. Growth of *mreB*$_{A325P}$ *C. crescentus* cells. Phase contrast images were collected every 15 minutes for 7.25 hours. Scale bar is 1 μm. Corresponds to Fig. 1A, right panel.

Movie S3. Venus-MreB$_{A325P}$ patches are dynamic and show circumferential movement. Epifluorescence images were collected every 8 seconds for 2 minutes and the movie is looped 6 times as indicated by timestamps. Arrow denotes a circumferentially moving patch analyzed by kymograph in Fig. S1. Images have been smoothed using a three-dimensional third-order Savitzky-Golay filter of dimension 5 pixels x 5 pixels x 5 frames to smooth noise and capture persistently moving spots. Images have also been normalized to correct for bleaching, inverted, and scaled up with interpolation for ease of viewing. Scale bar is 5 μm. Corresponds to Fig. S1.

Movie S4. Growth of an *mreB*$_{A325P}$ cell depleted of FtsZ. Phase contrast images were collected every 15 minutes for 7.25 hours. Scale bar is 5 μm. Corresponds to Fig. 5B-C.

Movie S5. Surface area to volume ratio trajectories of individual cells over time. Colors on the graph correspond to cell outline colors and when cells divide daughters are assigned new colors. Phase contrast images are the same as Movie S2 and the scale bar is 1 μm. Corresponds to Fig. 8A.

Supplementary Figures

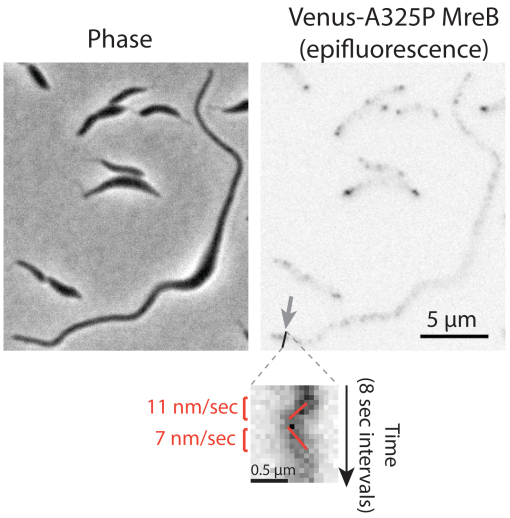

Fig. S1. Venus-MreB$_{A325P}$ patches show dynamic circumferential motion.
Epifluorescence images of A325P cells expressing Venus-MreB$_{A325P}$ were acquired every 8 seconds. One representative epifluorescence image is shown as well as a phase contrast image of the same field. The gray arrow indicates the line from which the kymograph, below, was taken. Red lines on the kymograph mark the trajectory of an MreB patch over time and the slopes of these lines were used to calculate approximate patch speeds, noted on the left. See also Movie S3.

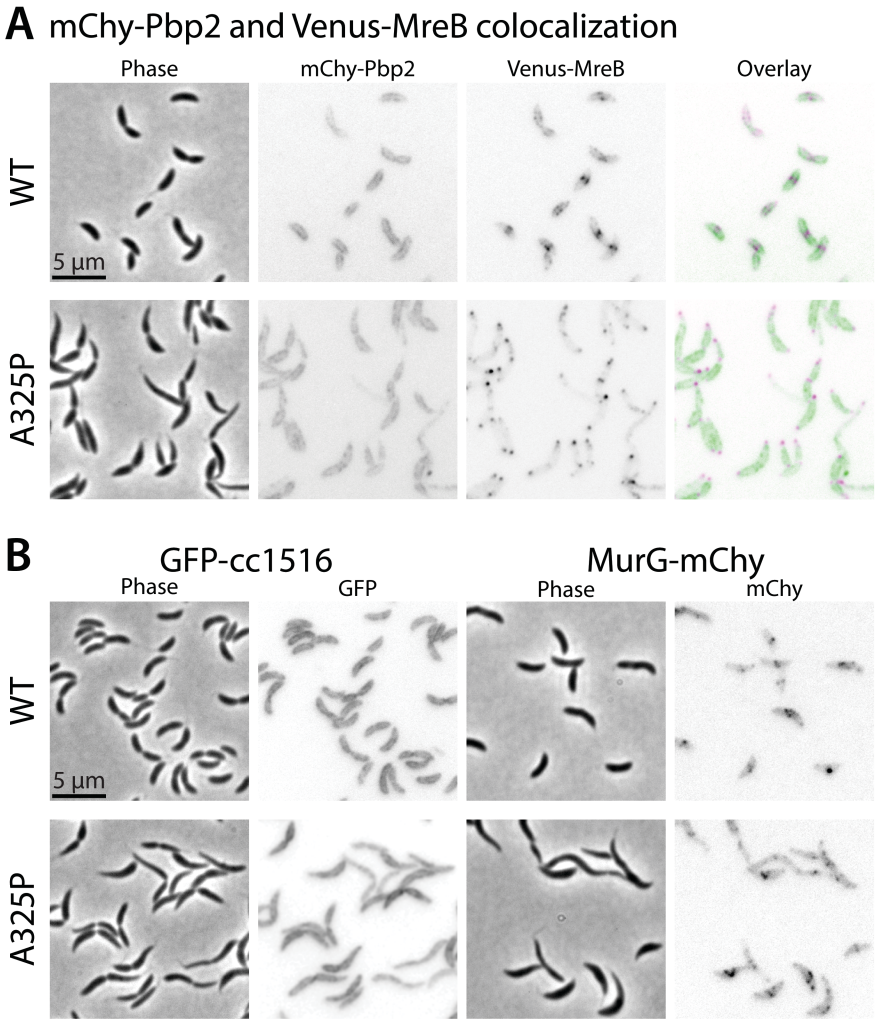

Fig. S2. $MreB_{A325P}$ does not alter the subcellular localization of the peptidoglycan synthesis machinery. A. Representative phase contrast and epifluorescence images of wild-type and *mreB*$_{A325P}$ cells expressing mCherry-Pbp2 (Hocking *et al.*, 2012) from the vanillate-inducible promoter and Venus-MreB (WT or A325P as labeled) from the xylose-inducible promoter.

B. Representative phase contrast and epifluorescence images of wild-type and *mreB*$_{A325P}$ cells expressing GFP-cc1516 (Hocking *et al.*, 2012) or MurG-mCherry (Goley *et al.*, 2010) from the xylose-inducible promoter. The localization patterns of MreC and Pbp3 were also found to be similar in wild-type and A325P cells (data not shown).

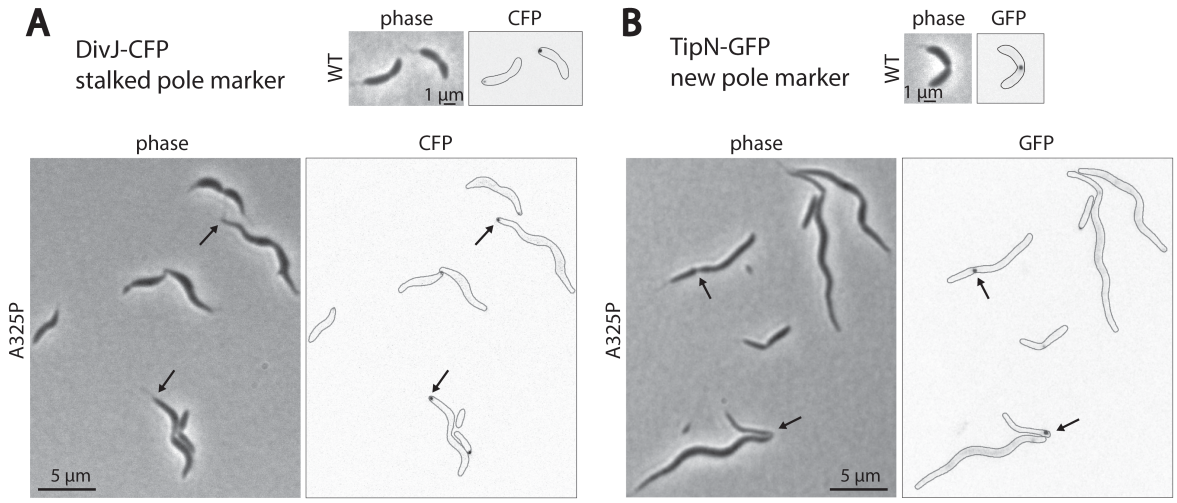

Fig. S3. Cell polarity is not disrupted in the *mreB*$_{A325P}$ mutant background.

A. Representative phase contrast and epifluorescence images of wild-type and *mreB*$_{A325P}$ cells expressing DivJ-CFP from the native DivJ locus (Wheeler and Shapiro, 1999). Arrows mark examples of DivJ foci localized to stalk poles.

B. Representative phase contrast and epifluorescence images of wild-type and *mreB*$_{A325P}$ cells expressing TipN-GFP from the native TipN locus (Huitema *et al.*, 2006). Arrows mark examples of TipN foci at new poles.

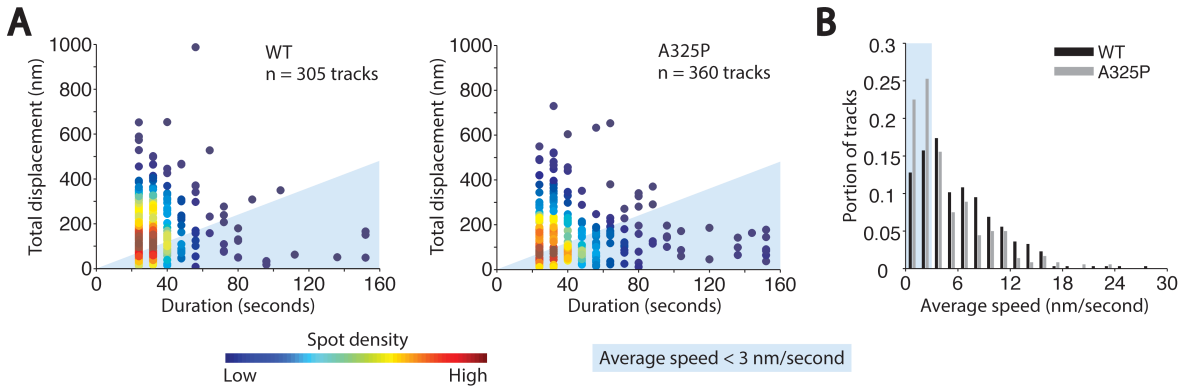

Fig. S4. A larger portion of automatically detected Venus-MreB$_{A325P}$ tracks were long-lived and immobile compared to wild-type.

A. Scatter plots of total displacement and duration of all automatically detected tracks in the wild-type and *mreB*$_{A325P}$ mutant backgrounds. Spot color signifies spot density and regions that are shaded blue correspond to displacement and duration values that give rise to average speeds of < 3 nm/second. This data is also shown in Fig. 4E-F.

B. Histogram of average speed for all automatically detected tracks. Blue shaded region again corresponds to tracks that are < 3 nm/second.

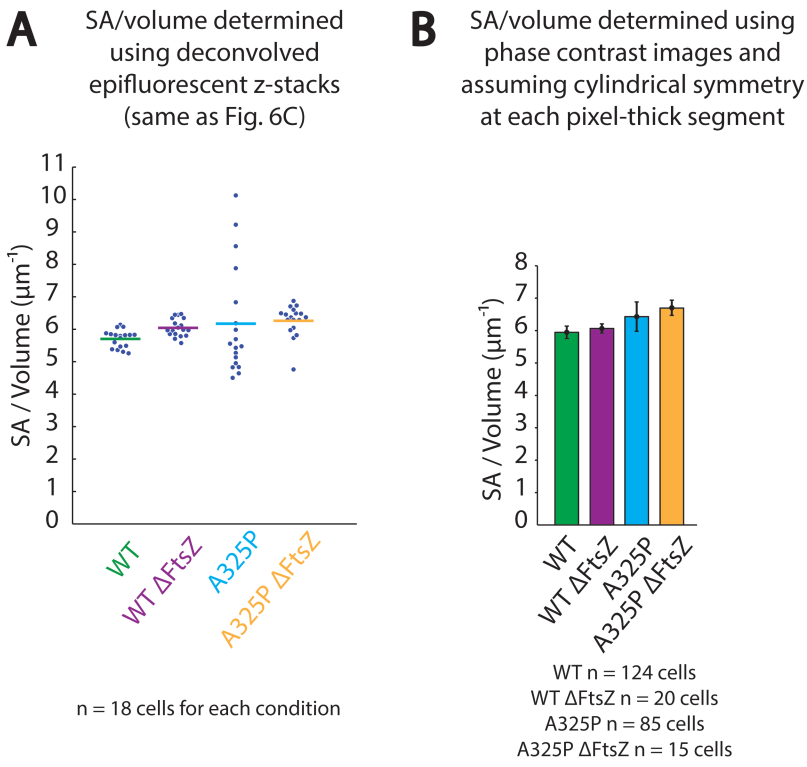

Fig. S5. Phase contrast and deconvolution methods of determining cell surface area to volume ratio give comparable results.

A. Plot of surface area to volume ratios of wild-type and *mreB*$_{A325P}$ cells with and without FtsZ determined using deconvolved epifluorescent z-stacks (same as Fig. 6C).

B. Bar graph of average surface area to volume ratio for the conditions in (A) determined using phase contrast microscopy and MicrobeTracker (Sliusarenko *et al.*, 2011) and assuming cylindrical symmetry for each pixel-thick segment along the cell axis. Bars represent the average surface area to volume ratio for n > 14 cells from each condition, and error bars represent the standard deviation.